Journal of the Korean Chemical Society
2012, *Vol. 56, No. 6*
Printed in the Republic of Korea
http://dx.doi.org/10.5012/jkcs.2012.56.6.679

Synthesis, Characterization and Biological Activities of 4-(*p*-Chlorophenyl)-1-(pyridin-2-yl)thiosemicarbazide and Its Metal Complexes

Mohammad M. Hassanien, Wael I. Mortada[†], Ali M. Hassan[‡], and Ahmed A. El-Asmy[§,*]

Chemistry Department, Industrial Education College, Beni-Suef University, Beni-Suef 62511, Egypt
[†]Clinical Chemistry Department, Urology and Nephrology Center, Mansoura University, Mansoura 35511, Egypt
[‡]Chemistry Department, Faculty of Science, Al-Azhar University, Cairo 11787, Egypt
[§]Chemistry Department, Faculty of Science, Mansoura University, Mansoura 35511, Egypt.
[*]E-mail: aelasmy@yahoo.com
(Received May 23, 2012; Accepted October 9, 2012)

ABSTRACT. New series of metal complexes of Co(II), Ni(II), Cu(II), Zn(II), Pd(II) and Pt(II) with 4-(*p*-chlorophenyl)-1-(pyridin-2-yl)thiosemicarbazide (HCPTS) have been synthesized and characterized by elemental analyses, magnetic moment, spectra (IR, UV-Vis, ^{1}H NMR, mass and ESR) and thermal studies. The IR data suggest different coordination modes for HCPTS which behaves as a monobasic bidentate with all metal ions except Cu(II) and Zn(II) which acts as a monobasic tridentate. Based on the electronic and magnetic studies, Co(II), Cu(II), Pd(II) and Pt(II) complexes have square - planner, Ni(II) has mixed stereochemistry (tetrahedral + square planar), while Zn(II) is tetrahedral. Molar conductance in DMF solution indicates the non-ionic nature of the complexes. The ESR spectra of solid copper(II) complex show $g_{\|}$ (2.2221) >$g_{\perp}$ (2.0899) > 2.0023 indicating square-planar structure and the presence of the unpaired electron in the $d_x2_{-y}2$ orbital with significant covalent bond character. The thermal stability and degradation kinetics of the ligand and its metal complexes were studied by TGA and DTA and the kinetic parameters were calculated using Coats–Redfern and Horowitz–Metzger methods. The complexes have more antibacterial activity against some bacteria than the free ligand. However, the ligand has high anticancer activities against HCT116 (human colon carcinoma cell line) and HEPG2 (human liver hepatocellular carcinoma cell line) compared with its complexes.

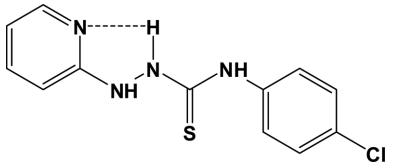
Key words: Metal complexes, 4-(*p*-chlorophenyl)-1-(pyridin-2-yl)thiosemicarbazide, Antibacterial and anticancer activities

INTRODUCTION

Thiosemicarbazides and their metal complexes have the subject of interest in coordination chemistry for their variable donor properties.[1] They form stable and intense colored complexes which are used for spectrophotometric determination of metal ions in different media[2-4] and showed catalytic activity.[5,6] Also, they have potentially beneficial as biological properties such as antibacterial,[7-10] antifungal,[7,9,10] antitumor,[11,12] antimalarial,[13] trypanocidal[14] and anti-inflammatory activities.[15]

Complexes of iron, cobalt, nickel, palladium and platinum with 2-hydrazinopyridine were reported;[16] the coordination sites were the pyridine ring and NH_2 group. 2-Hydrazinopyridine was found important in the synthesis of complexes used in the delivery of cytotoxin for therapy or the delivery of radionuclide for imaging and/or therapy. Diagnostic radiopharmaceuticals were used in majority of the diagnostic scans.[17,18] Schiff bases of 2-hydrazinopyridine with diacetylmonoxime,[19] 2,3-butanedione,[20] benzyl,[21] phenanthraquinone,[21] *o*-aminobenzaldehyde,[22] 1-isoquinolin-aldehyde,[23] 2-quinoxalinecarbox-aldehyde,[23] 2-thiophenealdehyde,[24] and 2, 9-diformylphenanthroline[25] were reported. Recently, 4-ethyl-1-(pyridin-2-yl)thiosemicarbazide and its Cu(II) complexes with different anions were synthesized, characterized[26] and used as a chelating agent for the separation, preconcentration, and determination of Cu(II) ions in saturated saline solutions by a cloud point extraction technique.[27] In addition, the complexes of 4-ethyl and 4-(*p*-tolyl)-1-(pyridin-2-yl)thiosemi-carbazides with Pd(II), Pt(II) and Ag(I)[28] showed antibacterial activity to some Gram positive and Gram negative bacterial strains.

Herein, we report the synthesis, characterization and biological activities of Co(II), Ni(II), Cu(II), Zn(II), Pd(II) and Pt(II) complexes of HCPTS (*Structure* 1).



***Structure* 1.** Structural formula of HCPTS.

EXPERIMENTAL SECTION

Materials

The metal salts and reagents used in this work: $CoCl_2 \cdot 6H_2O$, $NiCl_2 \cdot 6H_2O$, $CuCl_2$, $ZnCl_2$, $PdCl_2$, K_2PtCl_4, 2-hydrazinopyridine and 4-chlorophenyl-isothiocyanate were supplied from Aldrich and Fluka chemicals. The IR spectra, as KBr discs, were recorded using a Mattson 5000 FTIR Spectrophotometer. The electronic spectra, as DMF solution, were recorded on a Unicam UV–Vis Spectrophotometer UV2. The ^1H NMR spectra of HCPTS and its Pt(II), Pd(II) and Zn(II) complexes, in DMSO, were recorded on a EM-390 (200 MHz) Spectrometer. The mass spectra of the ligand and its metal complexes were recorded on 70 eV Shimadzu GC/MS – QP5050A instrument. The ESR spectrum of the Cu(II) complex was obtained on a Bruker EMX spectrometer working in the X-band (9.78 GHz) with 100 KHz modulation frequency. The microwave power was set at 0.001. The low field signal was obtained after 4 scans with a 10 fold increase in the receiver gain. A powder spectrum was obtained in a 2 mm quartz capillary at room temperature. Thermogravimetric analysis was performed using an automatic recording thermobalance type 951 DuPont instrument at heating rate 15 °C/min from room temperature to 800 °C in N_2. Carbon, hydrogen and nitrogen content of the ligand and its metal complexes were determined at the Microanalytical Unit, Cairo University, Egypt. The Cl^- content in the complexes was determined gravimetrically.[29] The Co(II), Ni(II), Cu(II) and Zn(II) analyses were carried out complexometrically according to the standard method.[29] Pd(II) and Pt(II) contents were determined using a Perkin Elmer flame atomic absorption spectrophotometer (Model AAnalyst 800); hollow cathode lamps for the investigated elements were used as spectral radiation sources (where λ = 247.6 and 265.9 nm and current = 30 and 15 for Pd(II) and Pt(II), respectively). The magnetic moment values were evaluated at room temperature (25±1 °C) using a Johnson Matthey magnetic susceptibility balance. The effective magnetic moments were calculated by applying:

$$\mu_{eff} = 2.828\sqrt{\chi_M T}$$

where χ_M is the molar susceptibility corrected using Pascal's constant for diamagnetism of all atoms in the complex and T is the absolute temperature. The molar conductance (10^{-3} M solutions) of the metal complexes, in DMSO, was measured on a HACH conductivity meter model Sens ion 5. All the measurements were taken at room temperature on freshly prepared solutions.

Preparation of HCPTS

HCPTS was prepared by heating under reflux a mixture of 2-hydrazinopyridine (0.1 mol) and 4-chlorophenylisothiocyanate (0.1 mol) in 20 ml absolute ethanol for 2 h. On cooling, fine white compound was formed, filtered off, washed with EtOH and Et_2O and recrystallized from EtOH (m.p. 175 C; yield 96%). The purity of the compound was checked by TLC.

Preparation of the Complexes

On mixing HCPTS (0.01 mol) in ethanol (20 mL) with 0.01 mol of the metal salt, precipitates were immediately formed. $PdCl_2$ and K_2PtCl_4 were dissolved in double distilled water in the presence of NaCl in case of $PdCl_2$. The reaction mixture was heated under reflux on a water bath for 2–3 h. On cooling, colored complexes were precipitated. They were filtered off, washed with ethanol then diethyl ether, dried and preserved in a vacuum desiccator over anhydrous calcium chloride.

Antibacterial Activities

The in vitro evaluation of antibacterial activity was performed against two bacterial strains, *Staphylococcus aureus* (Gram positive bacteria) and *Escherichia coli* (Gram negative bacteria). The bacterial species were grown in nutrient broth at 37 °C for 24 h.

The ligand and its metal complexes were tested on solid media using the diffusion technique.[30] Sterile diameter sensitivity discs (5 mm) were impregnated with different concentrations of the ligand or complexes in DMSO. Discs of each tested compound were laid onto nutrient agar for bacteria. Plates were surface spread with logarithmic phase bacterial cultures (0.2 mL). A spore suspension (108 spores/mL) for bacteria (0.5 mL) was also spread onto potato dextrose agar plates. The plates were then incubated for 24 h at 37 °C for bacteria. Antibiotic discs for Streptomycin were additionally tested as positive control. All determinations were performed in duplicate for each of the compounds. The average of two independent readings for each compound was recorded. The percentage inhibition in all of the replicates was calculated by the equation:

$$\% \text{ Inhibition} = \frac{(C-T)\times 100}{C}$$

Where C is the diameter of the microbial colony in the control plate and T is the diameter of the microbial colony in the test plate.

In Vitro Anticancer Activity

The antitumor assays were performed employing the following cell lines: HCT116 (human colon carcinoma cell line) and HEPG2 (human liver hepatocellular carcinoma cell line) according to the method of Skehan et al.[31] Human tumor cell lines were obtained frozen in liquid nitrogen from the American Type Culture Collection. The tumor cell lines were maintained in the National Cancer Institute, Cairo, Egypt, by serial sub-culturing.

Cells were used when 90% confluence was reached in T25 flasks. Adherent cell lines were harvested with 0.025% trypsin. Viability was determined by trypan blue exclusion using the inverted microscope (Olympus 1×70, Tokyo, Japan). Cells were seeded in 96-well microtiter plates at a concentration of 5×10^4–10^5 cell/well in a fresh medium and left to attach to the plates for 24 h. Then, the cells were incubated with the appropriate concentration ranges of compound under test dissolved in DMSO, completed to total of 200 μl volume/well using fresh medium and incubation was continued for 24, 48 and 72 h. Control cells were treated with vehicle alone. For each drug concentration, 4 wells were used. Following 24, 48 and 72 h treatment, the cells were fixed with 50 μl cold 50% trichloroacetic acid for 1 h at 4 °C. Wells were washed 5 times with distilled water and stained for 30 min at room temperature with 50 μl 0.4% Sulphorhodamine-B dissolved in 1% acetic acid. The wells were then washed 4 times with 1% acetic acid. The plates were air-dried and the dye was solubilized with 100 μl/well of 10 mM tris base (ph 10.5) for 5 min on a shaker (Orbital shaker OS 20, Boeco, Germany) at 1600 rpm. The optical density of each well was measured spectrophotometrically at 564 nm with an ELIZA microplate reader (Meter tech. Σ 960, U.S.A.). The mean background absorbance was automatically subtracted and the mean values of each concentration were calculated. The percentage of cell survival was calculated as follows:

Survival fraction = O.D. (treated cells)/O.D. (control cells)

The IC_{50} value was defined as the concentration of test sample resulting in a 50% reduction of absorbance as compared with untreated controls that received a serial dilution of the solvent in which the test samples were dissolved, and was determined by linear regression analysis. Doxorubicin was used as the standard.

RESULTS AND DISCUSSION

The color, melting point, elemental analysis and molar conductivity of the prepared complexes are listed in *Table* 1. The complexes are stable at air, non-hygroscopic and insoluble in water and most organic solvents, but soluble in DMSO and DMF; Ni(II) and Cu(II) complexes are partially soluble in DMSO and DMF and their molar conductances can not be measured. All complexes have melting points >300 °C; Cu(II) complex has 243 °C. The molar conductance values of 10^{-3} mol l^{-1} solutions in DMSO are in the range of 4.4-23.2 $Ohm^{-1}cm^2mol^{-1}$ indicating their nonelectrolytes.

IR Spectra

The most important IR bands of the ligand and its metal complexes together with their assignments are summarized in *Table* 2. Representative example for their spectra is given in *Fig*. 1.

The spectrum of HCPTS exhibits characteristic bands at 3262, 3172 and 3131 cm^{-1} attributed to $\nu(N^4H)$, $\nu(N^1H)$ and $\nu(N^2H)$, respectively.[26] The $\nu(C=N)_{Py}$ appearing as a strong band at 1598 cm^{-1}. The appearance of $(C=N)_{Py}$ and N^2H bands at lower values than those reported suggests intramolecular hydrogen bonding.[27] Also, the two bands at 1512 and 1290 cm^{-1} were assigned to thioamide I and III,[26]

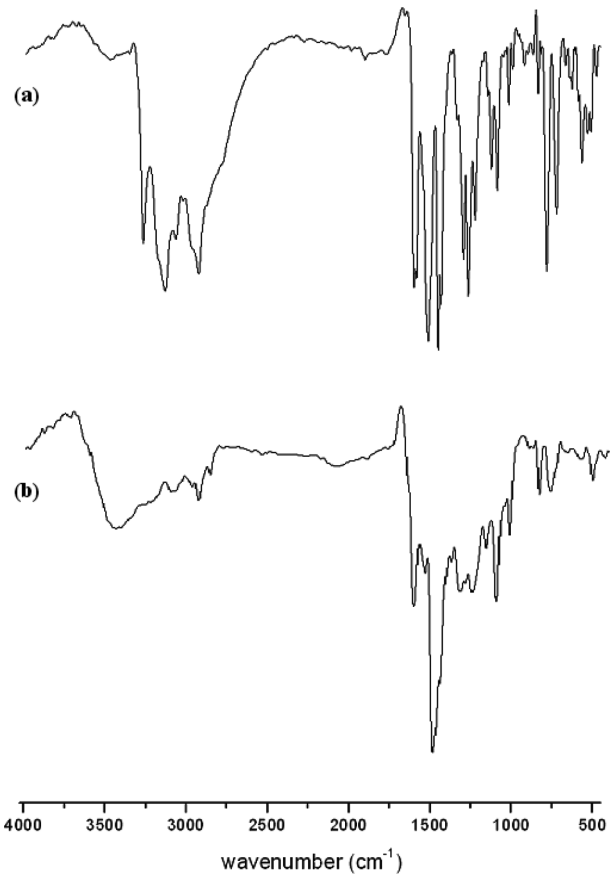


***Fig.* 1.** IR spectra of: (a) HCPTS and (b) [Co(CPTS)(H_2O)OH].

***Table* 1.** Physical properties and elemental analysis of HCPTS and its metal complexes

No.	Compound	Formula weight		Color	M.P. (ºC)	%Found					%Calculated				
		Found*	Calcd.			C	H	N	M	Cl	C	H	N	M	Cl
1	HCPTS	280.0	278.7	White	175	51.23	3.75	19.92	–	11.66	51.70	3.98	20.10	–	12.72
2	[Co(CPTS)(H_2O)OH]	371.6	371.6	Dark brown	>300	38.28	3.79	14.59	15.46	8.90	38.77	3.53	15.07	15.85	9.54
3	[Ni(CPTS)(H_2O)OH]	371.0	371.4	brown	>300	39.42	3.48	14.44	15.82	9.12	38.80	3.53	15.08	15.80	9.54
4	[Cu(CPTS)Cl]	376.5	376.5	Green	243	37.72	2.80	14.21	16.60	17.51	38.26	2.68	14.87	16.87	18.82
5	[Zn(CPTS)OH]	362.0	360.1	Brown	>300	41.26	2.94	15.45	18.35	9.65	39.98	3.05	14.93	18.10	9.86
6	[Pd(CPTS)(H_2O)Cl]	437.8	437.6	Dark brown	>300	32.68	2.51	12.09	22.90	15.62	32.93	2.76	12.80	24.32	16.20
7	[Pt(CPTS)(H_2O)Cl]	526.1	526.3	brown	>300	27.28	2.29	10.63	37.90	13.62	27.36	2.28	10.64	37.05	13.49

*Values obtained from mass spectra

***Table* 2.** Significant IR spectral data (cm^{-1}) of HCPTS and its complexes

Compound	ν(OH)	δ(OH)	ν(N^4H)	ν(N^1H)	ν(N^2H)	ν(C=N)$_{Py}$	ν($C=N^2$)	Thioamides I,II, III	ν(C=S)	ν(C–S)	in-plane deformation mode of the pyridine ring	ρ(NH)	ν(M–N)
HCPTS	–	–	3262 m	3172 sh	3131 s	1598 s	–	1512 s, 1294 s, 991 s	783 s	–	625 w	723 m	–
[Co(CPTS)(H_2O)OH]	3428 br	1314 br	3297 sh	3193 m	–	1599 s	1629 sh	1531 m, 1313 m, 1010 s	–	678 sh	624 w	730 sh	501 s
[Ni(CPTS)(H_2O)OH]	3320-3446 br	1310 w	3257 sh	3222 w	–	1594 s	1629 sh	1536 s, 1305 w, 1002 s	–	670 w	624 w	752 s	493 m
[Cu(CPTS)Cl]	–	–	3272 sh	3194 w	–	1589 s	1652 m	1521 w, 1305 m, 1004 s	–	674 w	650 w	755 sh	498 s
[Zn(CPTS)OH]	3432 br	1310 w	3289 sh	3195 sh	–	1617 m	1635 sh	1521 w, 1311 w, 1008 s	–	673 w	652 w	758 s	495 w
[Pd(CPTS)(H_2O)Cl]	3455 br	1311 w	3289 w	3210 sh	–	1598 s	1631 sh	1527 m, 1311 s, 1014 w	–	674 w	622 w	746 s	501 s
[Pt(CPTS)(H_2O)Cl]	3467 br	1310 w	3289 br	3222 br	–	1590 s	1633 w	1519 m, 1309 s, 1012 w	–	678 w	625 w	748 s	505 m

S=sharp, m=medium, w=weak, br=broad, sh=shoulder.

respectively. Moreover, two sharp bands at 783 and 723 cm^{-1} are attributed to ν(C=S) and ρ(NH).[28] No band observed in the range 2500-2600 cm^{-1} due to ν(SH)[28] indicating that the ligand exists in the thione form. A value of 625 cm^{-1} belongs to the in-plane deformation mode of the pyridine ring.[32]

On comparison of the spectra of [Co(CPTS)(H_2O)OH], [Ni(CPTS)(H_2O)OH], [Pd(CPTS)(H_2O)Cl] and [Pt(CPTS) (H_2O)Cl] with that of the ligand, the broad band centered at 3428 cm^{-1} is attributed to ν(OH) of the coordinated water and hydroxyl group,[33] another evidence for the presence of hydroxo OH is the appearance of a band at 1380 cm^{-1} attributed to OH bending vibration. The 3297-3257 and 3222-3193 cm^{-1} weak bands are assigned to ν(N^4H) and ν(N^1H), respectively.[33] The disappearance of ν(N^2H) and ν(C=S) with the appearance of new shoulders at 1629 and 678 cm^{-1} attributed to ν($C=N^2$) and ν(C-S), respectively[28] confirming the thiol form of the ligand. The shift of ν(N^1H) is due to its coordination to the metal ion. Thus, the N^1 and S atoms are the coordination sites. The limitation of our IR instrument (400-4000 cm^{-1}) prevents the appearance of ν(M-Cl) in the range 330-250 cm^{-1}.

In [Cu(CPTS)Cl] and [Zn(CPTS)OH], the ligand behaves as a mononegative tridentate coordinating through $C=N_{py}$, $C=N^1$ and C-S groups. In [Zn(CPTS)OH], the spectrum shows a broad band at 3432 cm^{-1} attributed to ν(OH). In the two complexes, the band appeared at 1635-1652 cm^{-1} is assigned to ν($C=N^2$).[26] The absence of ν(N^2H) and ν(C=S) confirming the thioenol form. The shift of ν(N^1H) and ν(C=N)$_{Py}$ indicates their involvement in the coordination. The shift in the in-plane deformation modes of the pyridine ring is another support of the participation of the pyridine nitrogen in the coordination.

^{1}H NMR Spectra

The ^{1}H NMR spectrum of the ligand and its Zn(II), Pd(II) and Pt(II) complexes were

***Table* 3.** ^{1}H NMR spectral data of HCPTS and its Zn(II), Pd(II) and Pt(II) complexes (ppm)

Compound	N^1H	N^2H	N^4H	H^3_{Py}	H^4_{Py}	H^5_{Py}	H^6_{Py}	H^2_{Bz}	H^3_{Bz}
HCPTS	9.79	8.54	9.91	6.66	7.59	6.82	8.14	7.18	7.36
[Zn(CPTS)OH]	10.78	–	9.4	6.62	7.62	6.95	8.38	7.17	7.32
[Pd(CPTS)(H_2O)Cl]	10.9	–	9.84	6.59	7.53	6.88	8.23	7.04	7.17
[Pt(CPTS)(H_2O)Cl]	10.57	–	9.8	6.58	7.59	6.83	8.59	7.23	7.38

recorded to confirm the binding mode of HCPTS towards the metal ions. The results are summarized in *Table* 3. Representative data are also shown in *Fig*. 2.

The ^{1}H NMR spectrum of HCPTS in DMSO-d_6 shows signals due to the protons of the phenyl and pyridine.[26] The three singlet signals at 9.79, 8.54 and 9.91 ppm are attributed to the N^1H, N^2H and N^4H protons, respectively. The other NH protons are shifted upfield due to the inductive effect of pyridyl and phenyl rings as electron donor groups.[27]

The spectra of Zn(II), Pd(II) and Pt(II) complexes, in DMSO-d_6 show the disappearance of the N^2H signal indicating the deprotonation of this group upon complexation and subsequent coordination through the thioenol form of the ligand. Also, the signal of N^1H was shifted downfield indication the corporation of this group in complexation.[27]

Electronic Spectra and Magnetic Moment

The electronic absorption spectral bands of the ligand and its metal complexes in DMF are reported in *Table* 4.

The absorption spectrum of HCPTS in DMF shows a band at 35715 cm^{-1} and three shoulders at 31250, 24390 and 23150 cm^{-1} attributing to $(\pi\rightarrow\pi^*)_{Py}$, $(\pi\rightarrow\pi^*)_{C=S}$, $(n\rightarrow\pi^*)_{Py}$ and $(n\rightarrow\pi^*)_{C=S}$.[26] The spectra of all complexes show two bands at 30490-32895 and 27935-29940 cm^{-1} due to $(\pi\rightarrow\pi^*)$ and $(n\rightarrow\pi^*)$ of the new $C=N^2$,[27] confirming the thioenol form of the ligand.

Co(II) complex (*Structure* 2) has a magnetic moment of 2.1 BM, which fall in the region reported for one unpaired electron existing in both square-planer and low spin octahedral geometries.[35] The absence of octahedral characteristic bands excludes the low spin octahedral configuration, whereas the broad band at 17600 cm^{-1} may assigned to $^1A_{1g}\rightarrow{}^1B_{1g}$ in a square-planer geometry.[34]

The Ni(II) complex exhibits two bands at 21550 and 14750 cm^{-1} (*Fig*. 3a) and magnetic moment of 2.2 BM. The data can be taken as evidence for the existence of mixed stereochemisty (tetrahedral + square planar). The first band is assigned to $^1A_{1g}\rightarrow{}^1B_{1g}$ in a square planer geometry while the second band is due to $^3T_1\rightarrow{}^1T_2$ in a tetrahedral geometry.[35]

The green Cu(II) complex shows a broad band centered at 12625 cm^{-1} which may be due to the envelope of transitions $^2B_{1g}\rightarrow{}^2A_{1g}$, $\rightarrow{}^2B_{2g}$, and $\rightarrow{}^2E_g$ suggesting a square planar geometry for the complex.[36] The other intense band at 25125 cm^{-1} may be assigned to LMCT (*Fig.* 3b). Its magnetic moment (0.54 BM) is below the expected value which is attributed to strong intermolecular copper-copper interaction and/or due to the covalent nature of metal-sulfur bond.[37]

The Zn(II) complex shows an absorption band at 25381 cm^{-1} attributed to the L to M charge transfer transition, which is compatible with this complex having a tetrahedral geometry.[38] The spectrum shows no bands in the region below 23000 cm^{-1} which is in accordance with the d^{10} electronic configuration of Zn(II).

The electronic spectra of the Pd(II) and Pt(II) (*Fig*. 3c) complexes showed three characteristic bands at 24750-24875, 23585-23150 and 18315-21550 cm^{-1} attributed to $^1A_{1g}\rightarrow{}^1A_{2g}$, $^1A_{1g}\rightarrow{}^1B_{1g}$ and $^1A_{1g}\rightarrow{}^1E_g$ transitions in square planer geometry[36] (*Structure* 3).

ESR Spectrum

The spin Hamiltonian parameters and the *G* value of the solid Cu(II) complex (S=1/2, I=3/2) are calculated. The ESR spectrum of the complex (*Fig.* 4) displayed axially symmetric *g*-tensor parameters with $g_{\|}$ (2.2221) > $g_{\perp}$ (2.0899) > 2.0023 indicating that the copper site has a $d_{x^2-y^2}$ ground state characteristic of square-planar or octahedral geometry.[39] In axial symmetry, the *g*-values are related to the *G*-factor by the expression $G = (g_{\|} - 2)/(g_{\perp} - 2)$. According to Hathaway,[40] if the value of G is greater than 4, the exchange interaction between Cu(II) centers in the solid state is negligible, whereas when it less than 4, a considerable exchange interaction exists in the solid complex. The G factor in [Cu(CPTS)Cl] is less than 4 (G = 2.47) suggesting copper-copper exchange interaction. The molecular-orbital coefficients, α^2 (a measure of the covalency of the in-plane σ-bonding between the 3d orbital and the ligand orbitals) and β^2 (the covalent in-plane π-bonding) were calculated employing the following equations:[41] $\alpha^2 = -(A_{\|}/0.036) + (g_{\|} - 2.0023) + 3/7(g_{\perp} - 2.0023) + 0.04$; $\beta^2 = (g_{\|} - 2.0023)E/-8\lambda\alpha^2$, where $\lambda = -828$ cm^{-1} for the free Cu(II) ion and E is the electronic transition energy. The lower value of α^2

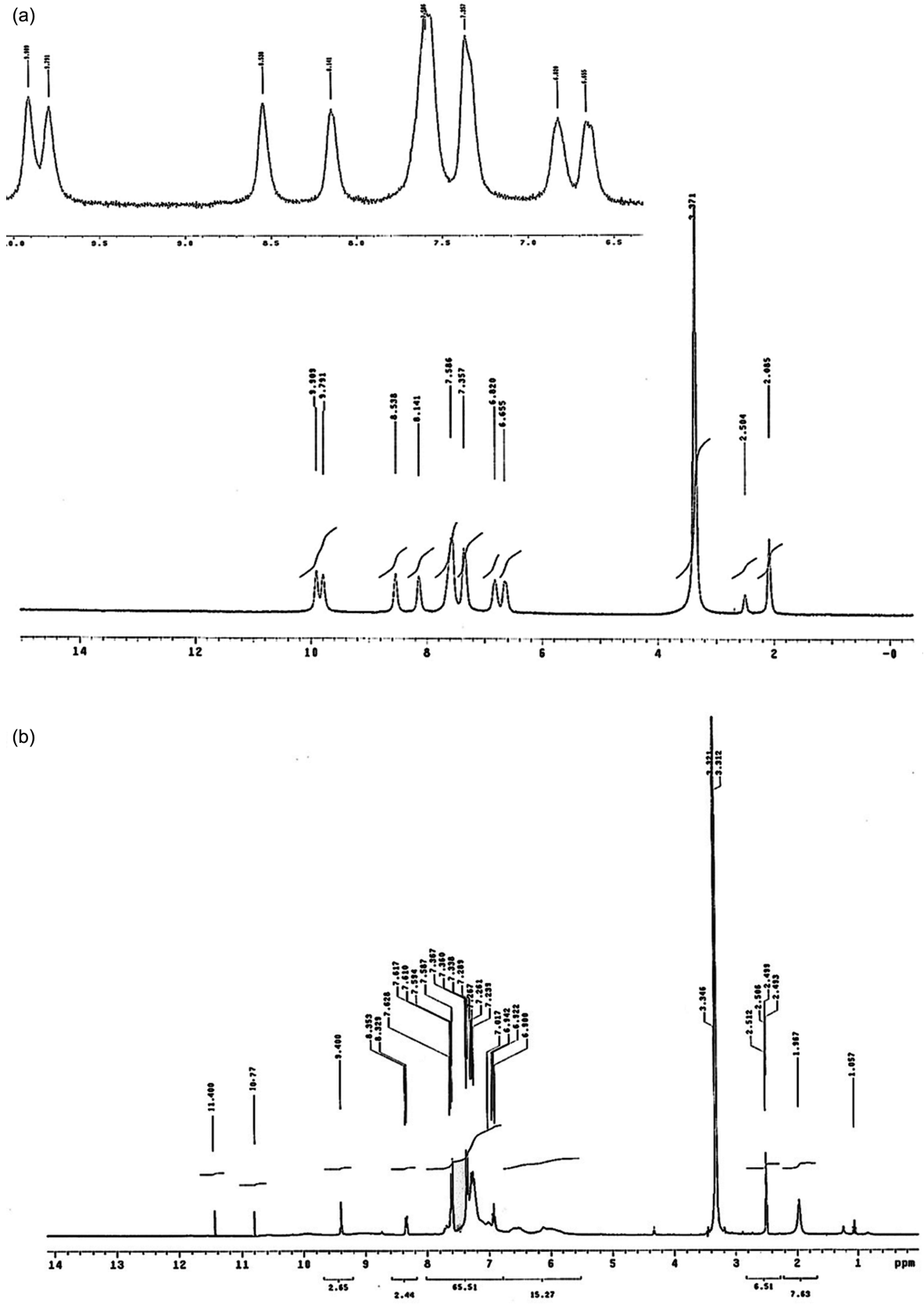
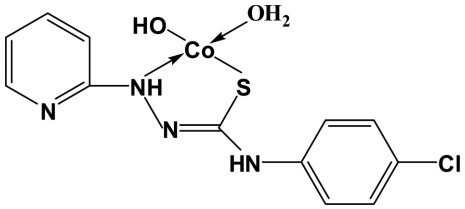


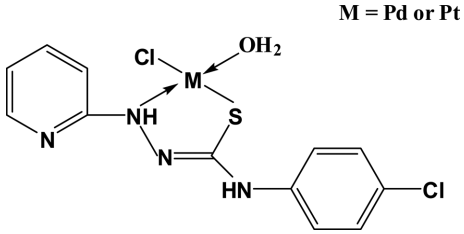
***Fig.* 2.** ^{1}H NMR of: (a) HCPTS and (b) [Zn(CPTS)OH].

***Table* 4.** Electronic spectral band and magnetic moment data of HCPTS and its metal ion complexes

Compound	Spectral bands, cm^{-1} (assignments)		μ_{eff} (BM)	Molar absorptivity (ε=$Lcm^{-1}mol^{-1}$)
	Intra-ligand	d-d transitions		
HCPTS	35714 $(\pi\rightarrow\pi^*)_{Py}$, 31250 $(\pi\rightarrow\pi^*)_{C=S}$, 24390 $(n\rightarrow\pi^*)_{Py}$ and 23148 $(n\rightarrow\pi^*)_{C=S}$	–	–	–
[Co(CPTS)(H_2O)OH]	35460 $(\pi\rightarrow\pi^*)_{Py}$, 31847 $(\pi\rightarrow\pi^*)_{C=N}{}^2$ and 29240 $(n\rightarrow\pi^*)_{C=N}{}^2$	23810 (LMCT) and 17600 ($^1A_{1g}\rightarrow{}^1B_{1g}$)	2.1	2460, 1190
[Ni(CPTS)(H_2O)OH]	35211 $(\pi\rightarrow\pi^*)_{Py}$, 32679 $(\pi\rightarrow\pi^*)_{C=N}{}^2$ and 29940 $(n\rightarrow\pi^*)_{C=N}{}^2$	21550 $^3T_1(F)\rightarrow{}^3T_1(P)$ and 14750 $^3T_1\rightarrow{}^lT_2$	2.2	2378, 1629
[Cu(CPTS)Cl]	34965 $(\pi\rightarrow\pi^*)_{Py}$, 30864 $(\pi\rightarrow\pi^*)_{C=N}{}^2$ and 28249 $(n\rightarrow\pi^*)_{C=N}{}^2$	12625 (overlap of $^2A_{1g}\rightarrow{}^2B_{1g}$ and $^2E_g\rightarrow{}^2B_{1g}$) and 25125 (LMCT)	0.54	1010, 1380
[Zn(CPTS)OH]	35714 $(\pi\rightarrow\pi^*)_{Py}$ and 30864 $(\pi\rightarrow\pi^*)_{C=N}{}^2$	25380 (LMCT)	–	
[Pd(CPTS)(H_2O)Cl]	35211 $(\pi\rightarrow\pi^*)_{Py}$, 32051 $(\pi\rightarrow\pi^*)_{C=N}{}^2$ and 27933 $(n\rightarrow\pi^*)_{C=N}{}^2$	24750 ($^1A_{1g}\rightarrow{}^1A_{2g}$), 23585 ($^1A_{1g}\rightarrow{}^1B_{1g}$) and 18315 ($^1A_{1g}\rightarrow{}^1E_g$)	–	
[Pt(CPTS)(H_2O)Cl]	35460 $(\pi\rightarrow\pi^*)_{Py}$, 31847 $(\pi\rightarrow\pi^*)_{C=N}{}^2$ and 29240 $(n\rightarrow\pi^*)_{C=N}{}^2$	24875 ($^1A_{1g}\rightarrow{}^1A_{2g}$), 23150 ($^1A_{1g}\rightarrow{}^1B_{1g}$) and 21550 ($^1A_{1g}\rightarrow{}^1E_g$)	–	



***Structure* 2.** The proposed structure of [Co(CPTS)(H_2O)(OH)].



***Structure* 3.** The proposed structure of [Pd(CPTS)(H_2O)Cl] and [Pt(CPTS)(H_2O)Cl].

(0.296) compared to β^2 (1.41) indicates that the σ-bonding in plane is more covalent than the in-plane π-bonding.[42]

Mass Spectra

The mass spectra of the ligand and its metal complexes confirmed the proposed formulae. The calculated and found molecular weights are given in *Table* 1. The mass spectrum of HCPTS (*Fig.* 5) shows its molecular ion peak at 280 [($C_{12}H_{11}N_4SCl$; MW = 278.7] and other peaks at 171, 111 and 77 may correspond to various fragments. The peak ascribed at 171 is assigned to $[C_7H_5NSCl]^+$ corresponding to the loss of $[C_5H_6N_3]^+$. The peak at 111 is corresponding to $[C_6H_4Cl]^+$ corresponding to the loss of $[CHNS]^+$. The peak at 77 represents the C_6H_4 with the loss of $1/2Cl_2$. The mass spectrum of [Co(CPTS)(H_2O)OH] (*Fig.* 6) shows the first peak at *m/z* 371.6 (Calcd. 371.6) representing the molecular ion peak (M^+) with 5.5% abundance. The base peak with m/e 169.5 represents the most stable fragment. For[Ni(CPTS)(H_2O)OH], the mass spectrum shows its molecular ion and base peaks at *m/z* 371.4 and 63.5, respectively. The molecular ion peaks of [Zn (CPTS)OH], [Pd(CPTS)(H_2O)Cl] and [Pt(CPTS)(H_2O)Cl] are observed at *m/z* = 360.0, 438.0 and 553.8, respec-

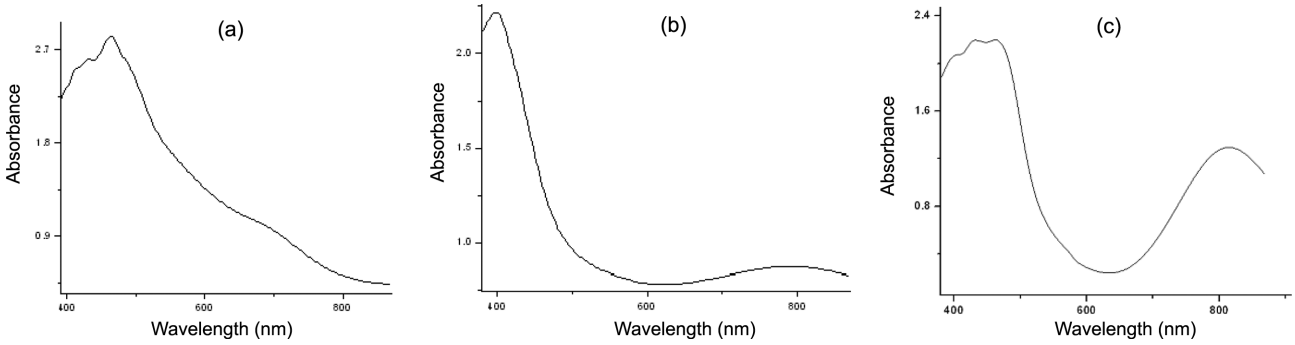


***Fig.* 3.** Absorption spectrum of (a) [Ni(CPTS)(H_2O)OH], (b) [Cu(CPTS)Cl], and (c) [Pt(CPTS)(H_2O)Cl].

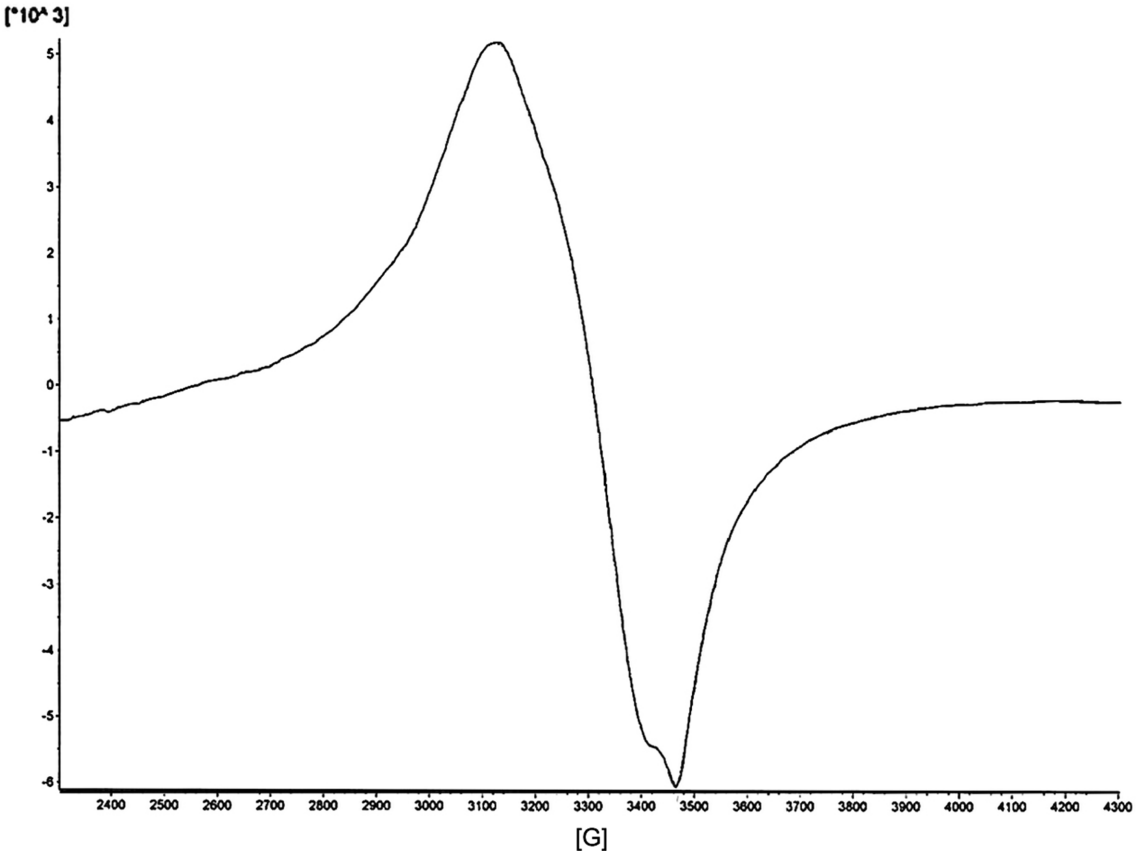


***Fig.* 4.** The ESR spectrum of [Cu(CPTS)Cl].

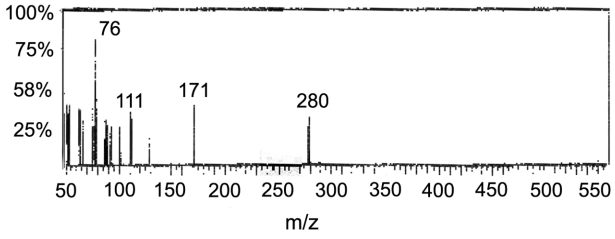


***Fig.* 5.** Mass spectrum of HCPTS.

tively. The mass spectra show series of peaks correspond to various fragments. Also, the base peaks were observed at $m/z = 78$ for each complex, supporting that the most abundant ion ($C_6H_5^+$) is similar for each complex. *Scheme* 1 demonstrates the proposed paths of the decomposition steps for the ligand and its Ni(II) and Zn(II) complexes.

Thermal Analysis and Thermodynamic Parameters

The TGA curve of HCPTS indicates a thermal stability till 167 °C coincident with its melting point (175 °C). The curve shows the first decomposition step (167 to 219 °C) corresponding to the loss of C_5H_4N and ClC_6H_4 (Found 68.2%; Calcd. 68%). The second (219 to 347) is attributed to the loss of N_3H_3 (Found 15.9%, Calcd. 16.1%), leaving a residue of C+S (Found 15.9%, Calcd. 15.8%). Comparing the TGA data (*Table* 5) of the ligand with those of the complexes, clearly support that the complexes showed high thermal stability where the starting point of the ligand decomposition in the complexes shifts to a higher temperature (°C).

In the TGA thermogram of [Co(CPTS)(H_2O)OH], the first stage at 186 °C with weight loss of 25.1% may be due to the loss of coordinated water and C_5H_4N (Found 25.1; Calcd. 25.8%). The second stage centered at 339 °C is corresponding to the elimination C_6H_4Cl (Found 29.5; Calcd. 29.97%). The final stage is due to the lost of NHNHCSNH (Found 24.4; Calcd. 24%) leaving a residue of CoO (Found 19.08: Calcd. 20.2%).

[Cu(CPTS)Cl] showed three steps of degradation. The first centered at 170 °C is corresponding to the loss of 1/2Cl_2 (Found 9.40; Calcd. 9.40%). The second step (230-480 °C) is attributed to the loss of C_6H_4N (Found 21.8; Calcd. 20.7%). The final stage (480-800 °C) is due to the loss of NHPhCl (Found 32.2; Calcd. 33.5%) leaving a stable residue of $CuCN_2S$ (Found 37.9; Calcd. 36.4%).

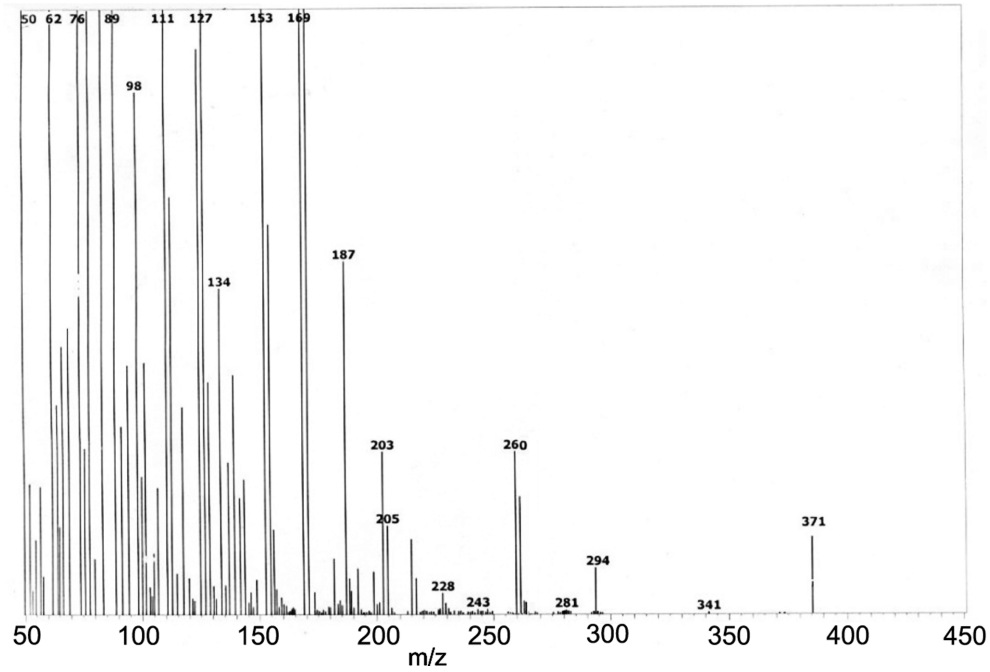
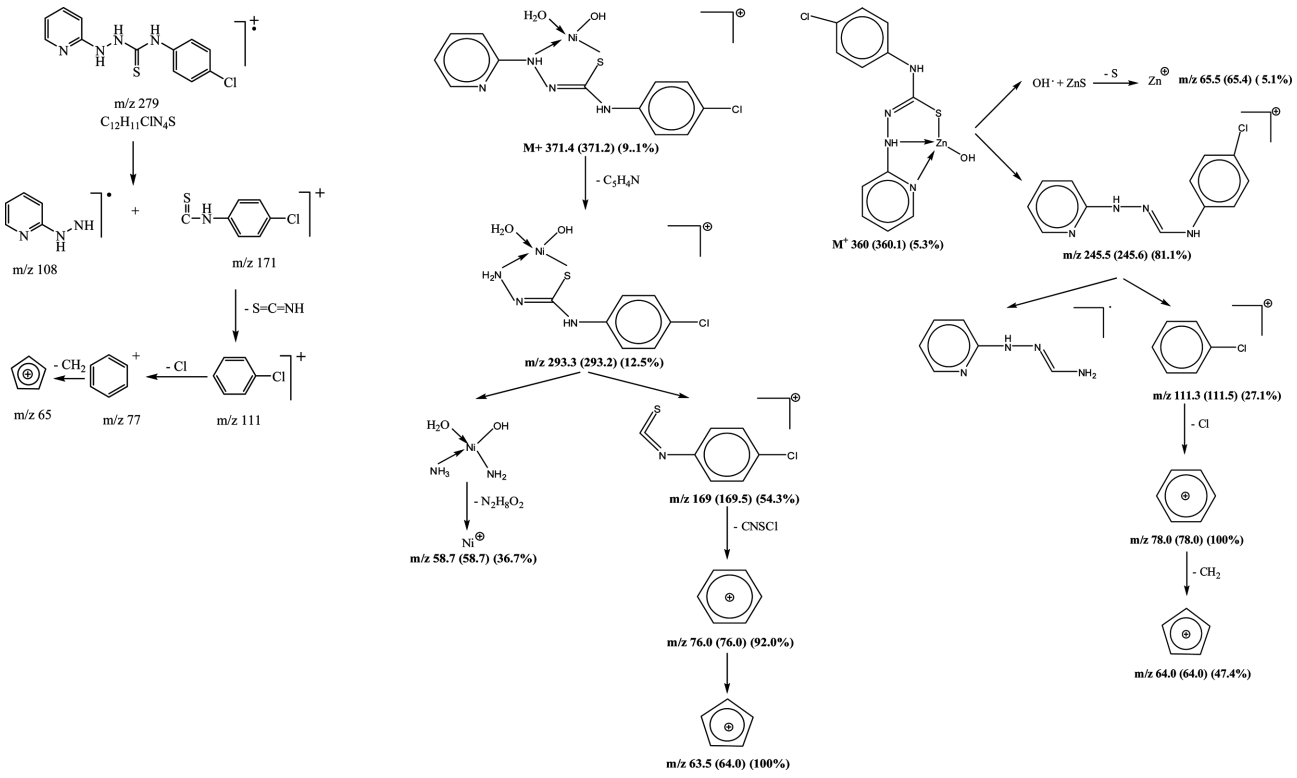


***Fig.* 6.** Mass spectrum of [Co(CPTS)(H_2O)OH].



***Scheme* 1.** The proposed fragmentation pattern for the ligand and its Ni(II) and Zn(II) complexes.

The TGA of [Zn(CPTS)OH] shows four stages for degradation. The first from 150 to 201 °C (centered at 169) is assigned for the removal of OH (Found 4; Calcd. 4.7%). The second centered at 314 °C is attributed to the loss of C_5H_4N (Found 20.13; Calcd. 21.6%). The third one (437–645 °C) is corresponding to the removal of C_4H_2Cl (Found

***Table* 5.** Thermal analysis data of HCPTS and its metal complexes

Compound	Temp. (°C)	Thermal analysis		Thermodynamic parameters					
		Wt loss%	Fragment removed, (Calcd.%)	E*	ΔS*	ΔH*	ΔG*	A	R
HCPTS	167-219	68.2%	$C_5H_4N + C_6H_4Cl$ (68%)	157(189)	−5.2	153	155	5.4×10^{12}	0.928
	219-347	15.9%	N_3H_3 (16.1%)	54(47)	−244	50	169	1.71	0.961
	Residue	15.9%	C + S (15.8%)	–	–	–	–	–	–
[Co(CPTS)(H$_2$O)OH]	117-274	25.1%	$H_2O + C_5H_4N$ (25.8%)	45.6(59)	−239	41.6	158	3.34	0.977
	274-438	29.5%	C_6H_4Cl (29.97%)	63(62.2)	−273	59	174	4.1	0.928
	438-584	24.4%	N_3H_3CS (24%)	107(103)	−223	103	212	22.8	0.991
	Residue	19.08%	CoO (20.2%)	–	–	–	–	–	–
[Ni(CPTS)(H$_2$O)OH]	114-178	5%	H_2O (4.8%)	75(61.6)	−170	71	154	13434	0.998
	178-335	53.7%	$C_5H_4N + C_6H_4Cl$ (53.9%)	72(81)	−212	68	171	84	0.939
	335-572	20.2%	N_3H_3CS (20.04%)	44.8(44.2)	−198.7	40.7	137.5	421.7	0.985
	Residue	20.2%	NiO (20.04%)	–	–	–	–	–	–
[Cu(CPTS)Cl]	100-230	9.40%	Cl (9.40%)	47(51)	−247.7	43	163.7	1.16	0.977
	230-480	21.8%	C_6H_4N (20.70%)	44.7(46.2)	−210.8	40.6	143.3	98.8	0.967
	480-800	32.2%	NHC_6H_4Cl (33.5%)	84(81)	−215	80	184.8	58	0.984
	Residue	37.9%	$Cu(CN_2S)$ (36.4%)	–	–	–	–	–	–
[Zn(CPTS)OH]	150-201	4%	OH (4.7%)	61.3(58)	−200	57	154.8	346	0.985
	201-437	20.13%	C_5H_4N (21.6%)	50.8(56)	−212	46.8	150	83.3	0.983
	437-645	22.51%	C_4H_2Cl (23.6%)	102(115)	−227	98.8	209	14	0.990
	645-788	8%	C_2H_2 (7.2%)	180(166)	−176.5	175.9	261.9	6103	0.977
	Residue	46.84%	$Zn(CH_4N_3S)$ (43.1%)	–	–	–	–	–	–
[Pd(CPTS)(H$_2$O)Cl]	145-257	12.27%	H_2O + Cl (12.2%)	81.9(75)	−183	77.8	167	2657	0.999
	257-374	17.2%	C_5H_4N (17.7%)	67.3(55.2)	−233	63.3	176.7	6.9	0.999
	374-466	38.4%	$C_6H_4Cl + CN_3H_3$ (38.4%)	263(243)	31.5	259	244	4.5	0.957
	Residue	29.8%	PdS (31.3%)	–	–	–	–	–	–
[Pt(CPTS)(H$_2$O)Cl]	159-378	10.1 %	H_2O + Cl (10.2%)	46(58.7)	−211	41.9	144.9	91.5	0.990
	378-592	14.9%	C_5H_4N (14.8%)	71.7(68)	−217.5	67.7	173.6	44	0.984
	592-770	21.6%	C_6H_4Cl (21.2%)	159(165)	-188	155	246	1544	0.970
	Residue	53.7%	$Pt(CN_3S)$ (53.5%)	–	–	–	–	–	–

*The values between brackets are calculated using Horowitz-Metzger equation.

22.51; Calcd. 23.6%). The final stage (645−788 °C) is for the removal of C_2H_2 (Found 8.0; Calcd. 7.2%) leaving a residue of [$Zn(CH_4N_3S)$] (Found 46.8; Calcd. 43.1%).

[Pt(CPTS)(H$_2$O)Cl] showed three steps of degradation. The first centered at 272 °C is corresponding to the loss 1/2Cl_2 and the coordinated water molecule (Found 10.1; Calcd. 10.2%). The second step (378-592 °C) is attributed to the loss of pyridine fragment (Found 14.9; Calcd. 14.8%). The final stage (592−770 °C) is due to the loss of C_6H_4Cl (Found 21.6; Calcd. 21.2%) leaving a residue which may consists of $Pt(CN_3S)$ (Found 53.7; Calcd. 53.5%).

The kinetic parameters were evaluated graphically by employing Coats Redfern and Horowitz-Metzger equations. The kinetics and thermodynamic parameters: activation energy (E_a), enthalpy (ΔH^*), entropy (ΔS^*) and free energy (ΔG^*) change of decomposition, are evaluated graphically by employing Coats-Redfern[43] (Equations 1 and 2) and Horowitz-Metzger[44] (Equations 3 and 4). The results were summarized in *Table* 5.

Coats-Redfern

For $n \neq 1$

$$\ln X = \ln\left[\frac{AR}{\beta E_a}\right] - \frac{E_a}{RT} \quad \text{where } X = \left[\frac{1-(1-\alpha)^{1-n}}{T^2(1-n)}\right] \quad (1)$$

For n = 1

$$\ln X = \ln\left[\frac{AR}{\beta E_a}\right] - \frac{E_a}{RT} \quad \text{where } X = \left[\frac{-\ln(1-\alpha)}{T^2}\right] \quad (2)$$

Horowitz-Metzger

For $n \neq 1$

$$\ln X = \ln\left[\frac{ART_s^2}{\beta E_a}\right] - \frac{E_a}{RT_s} + \frac{E_a\theta}{RT_s^2} \text{ where } X = \left[\frac{1-(1-\alpha)^{1-n}}{1-n}\right] \quad (3)$$

For $n = 1$

$$\ln X = \ln \frac{E_a \theta}{RT_s^2} \quad \text{where} \quad X = [-\ln(1-\alpha)] \tag{4}$$

Where $\alpha = (w_o\text{-}w_t)/(w_o\text{-}w_f)$, $\theta = T\text{-}T_s$, T_s is the T_G peak temperature; T the temperature corresponding to the weight loss Wt; β is the heating rate ($Kmin^{-1}$); A is the pre-exponential factor (min^{-1}); R is the gas constant (8.314 $Jmol^{-1}\,K^{-1}$) and n is the order parameter for the decomposition stage. The activation thermodynamic parameters are calculated by Eyring equations: $\Delta H^* = Ea - RT$, $\Delta S^* = R \ln[Ah/kT]$ and $\Delta G^* = \Delta H^* - T\Delta S^*$ where ΔH^* in KJ mol^{-1}, ΔS in J mol^{-1} K^{-1}, ΔG in KJ mol^{-1}, h and k are Plank and Boltzmann constants.[41] The data obtained (*Table* 5) indicated that:

· All decomposition stages showed a best fit for n = 1. The other values have no better correlation.

· The E_a are moderately similar applying the two methods.

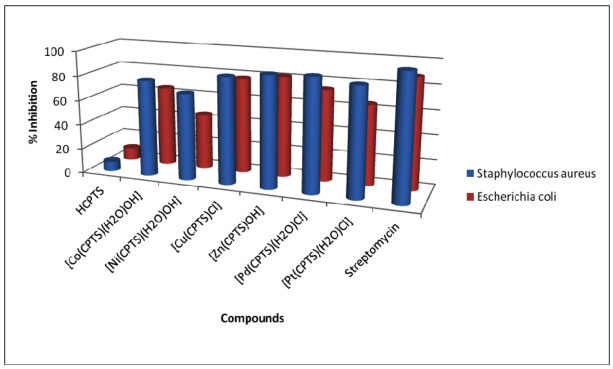
· The negative values of ΔS^* indicate that the activated fragments have more ordered structure than the undecomposed complexes and/or the decomposition reactions are slow.[45]

· The positive sign of ΔH^* reveals that the decomposition stages are endothermic processes.

· The positive sign of ΔG^* indicates that the free energy of the final residue is higher than that of the initial compound, and hence all the decomposition steps are non-spontaneous processes. Moreover, the values of ΔG^* increase significantly for the subsequent decomposition stages of a given compound. This conclusion, as a result of the increasing of $T\Delta S$, reflects that the rate of removal of the subsequent species is lower than that of the precedent one.[46] This may be attributed to the structural rigidity of the remaining complex after the expulsion of one or more fragment, as compared with the precedent complex, which requires more energy, $T\Delta S$, for its rearrangement before undergoing any decompositional change.

Antibacterial Activity

The antibacterial activity of HCPTS and its metal complexes were studied against *Staphylococcus aureus* and *Escherichia coli.* The diameter of the zone of inhibition is read 24 h after incubation at 37 °C. Antimicrobial activity was estimated on the basis of the size of the zone of inhibition formed around the paper disks on the plates. Streptomycin was used as a standard. The results in *Fig.* 7 show that the complexes exhibit inhibitory effects towards the activity of the selected species in contrast to the parent organic ligand which is less active under the experimental conditions. The increased lipophilic character of these complexes seems to be responsible for their enhanced potent antibacterial activity. It may be suggested that these complexes deactivate various cellular enzymes, which play a vital role in various metabolic pathways of these microorganisms. It has also been proposed that the ultimate action of the toxicant is the denaturation of one or more proteins of the cell, which as a result, impairs normal cellular processes.[47]



* *The concentration used is 50μg/disc.*

***Fig.* 7.** Antimicrobial activity of HCPTS and its metal complexes*.

In Vitro Anticancer Activity

HCPTS and its metal complexes have been tested against two human cancer cell lines: HCT116 and HEPG2. The IC_{50} values for these compounds were compared to Doxorubicin, an anticancer agent used nowadays. The result in *Fig.* 8 implies that HCPTS has more cytotoxic activity against the selected tumor cell lines compared with its metal complexes. Moreover, the IC_{50} of HCPTS is comparable with Doxorubicin. The antitumor efficacy of HCPTS may be attributed to its binding to cellular Fe pools. This

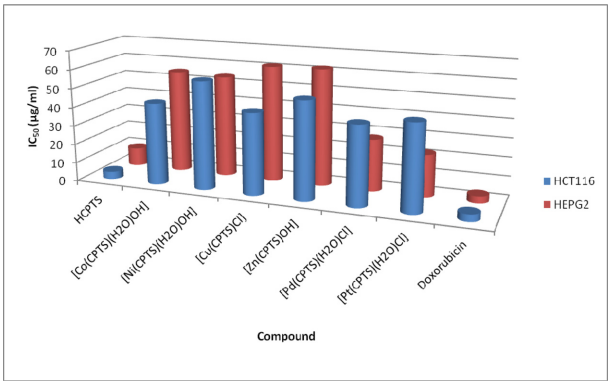


***Fig.* 8.** Cytotoxicity of HCPTS and its metal complexes against HCT116 and HEPG2 cell lines.

inactivates ribonucleotide reductase, the enzyme that catalyzes the conversion of ribonucleotides to deoxyribonucleotides. A strong positive correlation was established between RR activity and the rate of replication of tumour cells. The inhibition of RR prevents the production of deoxyribonucleotides. As a consequence these compounds interfere with DNA synthesis, thus decreasing the rate of replication of tumour cells and inhibiting tumour growth. The antitumour activity seems to be due to an inhibition of DNA synthesis in cancer cells produced by modification in reductive conversion of ribonucleotides to deoxyribonucleotides.[48]

CONCLUSION

The chemical and physical studies proved a square - planner structure for [Co(CPTS)(H_2O)OH], [Cu(CPTS)Cl], [Pd(CPTS)(H_2O)Cl] and [Pt(CPTS)(H_2O)Cl], mixed stereochemistry (tetrahedral + square planar) for [Ni(CPTS)(H_2O)OH] and tetrahedral for [Zn(CPTS)OH]. The metal complexes were biologically active against *Staphylococcus aureus* and *Escherichia coli*. HCPTS is a promising anticancer agent against HCT116 and HEPG2 cell lines.

REFERENCES

1. Gingras, B. A.; Somorjai, R. L.; Bayley, C. H. *Can. J. Chem.* **1961**, *39*, 973.
2. West, D. X.; Liberta, A.; Padhye, S. B.; Chikate, R. C.; Sonawane, P. B.; Kumbhar, A. S.; Yerande, R. G. *Coord. Chem. Rev.* **1993**, *123*, 49.
3. Akl, M. A.; Ismael, D. S.; El-Asmy, A. A. *Microchem. J.* **2006**, *83*, 61.
4. Saad, E. M.; El-Shahwai, M. S.; Saleh, H; El-Asmy, A. A. *Transition Met. Chem.* (Dordrecht, Neth.) **2007**, *32*, 155.
5. Hamada, M. M.; Shallaby, A. M.; El-Shafai, O.; El-Asmy, A. A. *Transition Met. Chem.* (Dordrecht, Neth.) **2006**, *31*, 522.
6. Hamada, M. M.; El-Shafai, O.; El-Asmy, A. A. *Transition Met. Chem.* (Dordrecht, Neth.) **2006**, *31*, 714.
7. Raman, N.; Selvan, A.; Manisankar, P. *Spectrochim. Acta, Part A* **2010**, *76*, 161.
8. Angelusiu, M. V.; Almajan, G. L.; Rosu, T.; Negoiu, M.; Almajan, E. R.; Roy, J. *Eur. J. Med. Chem.* **2009**, *44*, 3323.
9. Gulea, A.; Poirier, D.; Roy, J.; Stavila, V.; Bulimestru, I.; Tapcov, V.; Birca, M.; Popovschi, L. *J. Enzyme Inhib. Med. Chem.* **2008**, *23*, 806.
10. Chandra, S.; Gupta, L. K. *Sangeetika. Spectrochim. Acta, Part A* **2005**, *62*, 453.
11. Sathisha, M. P.; Budagumpi, S.; Kulkarni, N. V.; Kurdekar, G. S.; Revankar, V. K.; Pai, K. S. *Eur. J. Med. Chem.* **2010**, *45*, 106.
12. Vrdoljak, V.; Dilović, I.; Rubcić, M.; Kraljević Pavelić, S.; Kralj, M.; Matković-Calogović, D.; Piantanida, I.; Novak, P.; Rozman, A.; Cindrić, M. *Eur. J. Med. Chem.* **2010**, *45*, 38.
13. Bhat, A. R.; Athar, F.; Van Zyl, R. L.; Chen, C. T.; Azam, A. *Chem. Biodivers.* **2008**, *5*, 764.
14. Vieites, M.; Otero, L.; Santos, D.; Toloza, J.; Figueroa, R.; Norambuena, E.; Olea-Azar, C.; Aguirre, G.; Cerecetto, H.; González, M.; Morello, A.; Maya, J. D.; Garat, B.; Gambino, D. *J. Inorg. Biochem.* **2008**, *102*, 1033.
15. Berk, B.; Aktay, G.; Yesilada, E.; Ertan, M. *Pharmazie* **2001**, *56*, 613.
16. Edwards, D. A.; Larter, S. J. *Polyhedron* **1986**, *5*, 1213.
17. Blower, P. J.; Dilworth, J. R.; Maurer, R. I.; Mullen, G. D.; Reynolds, C. A.; Zheng, Y. *J. Inorg. Biochem.* **2001**, *85*, 15.
18. Banerjee, S. R.; Maresca, K. P.; Francesconi, L.; Valliant, J.; Bbich, J.W.; Zubieta, J. *Nucl. Med. Biol.* **2005**, *32*, 1.
19. Ibrahim, K. M.; Bekheit, M. M.; Abu El-Reash, G. M. *Transition Met. Chem.* **1991**, *16*, 189.
20. Chiswell, B. *Inorg. Chim. Acta* **1980**, *41*, 165.
21. Chiswell, B.; Lions, F.; Tomlinson, M. L. *Inorg. Chem.* **1964**, *3*, 492.
22. Chiswell, B.; Crawford, J. P.; O'Reily, E. J. *Inorg. Chim. Acta* **1980**, *40*, 223.
23. Case, F. H.; Schilt, A. A.; Simonzadeh, N. *Anal. Chem.* **1984**, *56*, 2860.
24. Sanchez, F. G.; Lopez, M. H. *Analyst* **1985**, *110*, 1253.
25. Carcelli, M.; Ianelli, S.; Pelagatti, P.; Pelizzi, G.; Rogolino, D.; Solinas, C.; Tegoni, M. *Inorg. Chim. Acta* **2005**, *358*, 903.
26. Hassanien, M. M.; Gabr, I. M.; Abdel-Rhman, M. H.; El-Asmy, A. A. *Spectrochim. Acta, Part A* **008**, *71*, 73.
27. El-Asmy, A. A.; Hassanien, M. M.; Abdel-Rhman, M. H.; Gabr, I. M. *J. Sulfur Chem.* **2010**, *31*, 141.
28. Hassanien, M. M.; Abdel-Rhman, M. H.; El-Asmy, A. A. *Transition Met. Chem.* **2007**, *32*, 1025.
29. Vogel, A. I. *A Text Book of Quantitative Inorganic Analysis*; Longmans: London, 1994.
30. William, H.; Stephen, V. *Theory and Application of Microbiological Assays*; Academic Press: San Diego, 1989.
31. Skehan, P.; Storeng, R.; Scudiero, D.; Monks, A.; McMahon, J.; Vistica, D.; Warren, J.T.; Bokesch, H.; Kenney, S.; Boyd, M. R. *J. Natl. Cancer Inst.* **1990**, *82*, 1107.
32. Yousef, T. A.; El-Gammal, O. A.; Ghazy, S. E.; Abu El-Reash, G. M. *J. Mol. Struct.* **2011**, *1004*, 271.
33. El Asmy, A. A.; Al-Gammal, O. A.; Saad, D. A.; Ghazy, S. E. *J. Mol. Struct.* **2009**, *934*, 9.
34. El-Metwally, N. M.; Gabr, I. M.; El-Asmy, A. A. *Transition Met. Chem.* **2006**, *31*, 71.
35. Abou-Hussen, A. A.; El-Metwally, N. M.; Saad, E. M.; El-Asmy, A. A. *J. Coord. Chem.* **2005**, *58*, 1735.
36. Lever, A. B. P. *Inorganic Electronic Spectroscopy*, 2nd ed.; Elsevier: Amsterdam, 1984.

37. Sawant, D. C.; Deshmukh, R. G. *J. Chem. Pharm. Res.* **2011**, *3*, 464.
38. Temel, H.; Ilhan, S.; Sekerci, M.; Ziyadanogullari, R. *Spectrosc. Lett.* **2002**, *35*, 219.
39. Speie, G.; Csihony, J.; Whalen, A. M.; Piepont, C. G. *Inorg. Chem.* **1996**, *35*, 3519.
40. Hathaway, B. J. *Struct. Bonding (Berlin)* **1984**, *57*, 55.
41. Jeyasubramanian, K.; Samath, S. A.; Tambidurai, S.; Murugesan, R.; Ramalingam, S. K. *Transition Met. Chem.* **1995**, *20*, 76.
42. Al-Hazmi, G. A. A.; El-Shahawi, M. S.; Gabr, I. M.; El-Asmy, A. A. *J. Coord. Chem.* **2005**, *58*, 713.
43. Coats, A. W.; Redfern, J. P. *Nature* **1964**, *201*, 68.
44. Horowitz, H. H.; Metzger, G. *Anal. Chem.* **1963**, *35*, 1464.
45. Frost, A. A.; Pearson, R. G. *Kinetics and Mechanisms*; Wiley: New York, 1961.
46. Kandil, S. S.; El-Hefnawy, G. B.; Baker, E. A. *Thermochim. Acta* **2004**, *414*, 105.
47. Agarwal, R.K.; Sharma, D.; Singh, L.; Agarwal, H. *Bioinorg. Chem. Appl.* **2006**, *2006*, 1.
48. Hu, W. X.; Zhou, W.; Xia, C.; Wen, X. *Bioorg. Med. Chem. Lett.* **2006**, *16*, 221.